Int. J. Electrochem. Sci., 9 **(2014)** 7986 - 7996

International Journal of
ELECTROCHEMICAL
SCIENCE
www.electrochemsci.org

Novel Three-dimensional Hierarchical Flower-like NiO-Co_3O_4 Composites as High-performance Electrode Materials for Supercapacitors

Peipei Liu, Zhonghua Hu[*], *Yafei Liu, Mingming Yao, Qiang Zhang, and Zijie Xu*

Department of Chemistry, Tongji University, 1239 Siping Road, Shanghai 200092, PR China
[*]E-mail: huzh@tongji.edu.cn

Received: 25 September 2014 / *Accepted:* 22 October 2014 / *Published:* 28 October 2014

In the present work, novel three-dimensional (3D) hierarchical NiO-Co_3O_4 composites are prepared by a facile and template-free hydrothermal method with L-lysine as the chelating agent. The flower-like NiO-Co_3O_4 composites display a high specific surface area and desirable pore distribution. The electrochemical performances are investigated by cyclic voltammetry, galvanostatic charge-discharge, and cycle life. The results reveal that the novel NiO-Co_3O_4 composites exhibit a high specific capacitance of 1988.6 F g^{-1} at 1 A g^{-1} and 1491.4 F g^{-1} at 15 A g^{-1}. Furthermore, the composites show an excellent cycling performance and stability with capacity retention of 94.0 % after 1500 cycles at 10 A g^{-1}. The outstanding capacitive behaviors are ascribed to the desirable composition and the unique 3D hierarchical flower-like structure.

Keywords: supercapacitors; NiO-Co_3O_4 composites; electrode materials; hierarchical flower-like; L-lysine

1. INTRODUCTION

Supercapacitors (also known as electrochemical capacitors or ultracapacitors) have attracted considerable attention due to their high specific power and energy density, fast charge and discharge rates, and long cycle life [1-4]. Therefore, they have great potential in many applications, such as in portable electronics, power back-ups, and electrical vehicles [5,6]. Generally speaking, the performance of supercapacitors strongly depends on the inherent properties of electrode materials [7-9]. To date, transition-metal oxides (TMOs), such as MnO_2 [10,11], NiO [12,13], Co_3O_4 [14,15] and V_2O_5 [16,17] *etc*. can be described as "always welcoming" candidates, because they possess multiple accessible valence states, which could enable a variety of reversible redox reactions and thus generate high pseudocapacitance [18]. Especially, NiO and Co_3O_4 have received tremendous interest due to

their controllable size and morphology, high theoretical capacity (2584 F g^{-1} and 3560 F g^{-1}, respectively), good electronic conductivity and favorable capacitive characteristics [19,20]. Huang *et al*. prepared NiO nanosheet arrays on Ni foam, which have a specific capacitance of 674.2 F g^{-1} at 1 A g^{-1} [21]. Yuan *et al*. reported the electrodeposited Co_3O_4 film *via* an electrodeposition, showing a specific capacitance of 443 F g^{-1} at 2 A g^{-1} [22]. However, these reported specific capacitances are much lower than their theoretical values.

Recently, in order to improve the specific capacitance of supercapacitors, combining different TMOs to form multi-component materials, which have two orders higher than all individual constituents, has been widely explored [23-26]. The investigations manifested that the morphology of the electrode materials also plays an important role in the electrochemical process. Noticeably, 3D hierarchical porous structures, which can provide smooth pathways for electrolytic ions and electrons to the active surfaces, have attracted much attention [27,28]. Fan *et al.* reported that Co_3O_4/NiO core/shell prepared by hydrothermal and chemical bath deposition methods, showing a specific capacitance of 853 F g^{-1} at 2 A g^{-1} [29]. Xu *et al*. fabricated hierarchical $NiCoO_2$ using polymeric nanotubes as template, displaying relatively high specific capacitance of 1468 F g^{-1} at 2 A g^{-1} [30]. Zhang *et al.* prepared mesoporous $NiCo_2O_4$ with 1619.1 F g^{-1} at 2 A g^{-1}, while 571.4 F g^{-1} at 10 A g^{-1} [31]. Although better capacitive behaviors have been achieved, the fabrication processes including deposition growth and template assist are complicated. Moreover, the specific capacitances are still low, especially at high current density. Therefore, further improvement is necessary.

In this work, hybrid-transition metal oxide of NiO-Co_3O_4 composites were designed and prepared by two-step process of template-free hydrothermal method combined with subsequent calcination, in which L-lysine was used as chelating agent to control the structure of the composite. Herein, a novel 3D hierarchical porous flower-like NiO-Co_3O_4 composite was obtained. The influence of calcination temperature on the properties of the composite was studied. The results showed that the NiO-Co_3O_4 composites displayed remarkable capacitive behaviors with superior specific capacitance, excellent rate capability and long term stability.

2. EXPERIMENTAL

2.1 Preparation of NiO-Co_3O_4 composites

Nickel sulfate hexahydrate ($NiSO_4 \cdot 6H_2O$), cobalt sulfate heptahydrate ($CoSO_4 \cdot 7H_2O$), L-lysine and sodium sulphate anhydrous (Na_2SO_4) were purchased from Aldrich. All reagents were of analytical grade and used without further purification. In a typical experiment, 5 mmol $NiSO_4 \cdot 6H_2O$, 5 mmol $CoSO_4 \cdot 7H_2O$, 2.0 g Na_2SO_4 and 10 mmol L-lysine were dissolved into 80 mL double distilled water in turn at room temperature and then stirred continuously for 30 min. The mixed solution was transferred into the Teflon-lined stain-less steel autoclave and maintained at 100 °C for 24 h. After cooling down to room temperature, the precipitate was separated by centrifugation, washed with double distilled water for several times, and dried at 70 °C for 12 h. Finally, the dried precipitate was calcinated at 350 °C for 4 h in air to obtain the final product. The influence of calcination temperature

on the properties of the composite was investigated. Besides, the finally products obtained at the temperature of 300, 350, 400 °C were denoted as T1, T2, T3, respectively.

2.2 Characterizations and measurements

The elemental compositions were investigated employing Energy Disperse Spectroscopy (EDS, 200kv). Crystal structure was analyzed by X-ray diffraction (XRD, D/max250VB3+/PC, Rigaku) equipped with Cu Kα radiation (0.15416 nm) from 10º to 90º. Field-emission scanning electron microscopy (FE-SEM, Hitachi S-4800 and JEOL JSM-6060) was used to study the morphology. The specific surface area and pore size distribution of prepared samples were estimated based on N_2 adsorption/desorption isotherms at 77 K (Micromeritics, Tristar3000 gas adsorption analyzer).

Electrochemical measurements were carried out on an electrochemical work station (CHI660C, Chenghua Shanghai). The NiO-Co_3O_4 composite as working electrode was prepared by mixing the active material, carbon black and polytetrafluoroethylene (PTFE) binder in the mass ratio of 8:1:1. A small amount of ethanol was added into the mixture and stirred by ultrasonic to form a homogeneous paste. After ethanol was evaporated, pressed the mixture into a sheet of 1 mm in thickness, then cut into some small wafers using a hole puncher. The wafers were dried at 70 °C for 12 h, and then pressed on a Ni grid at 20 MPa. Cyclic voltammetry (CV), galvanostatic charge-discharge test, and electrochemical impedance spectroscopy (EIS) were performed using conventional three-electrode system in 6 mol L^{-1} KOH aqueous solution as electrolyte. Hg/HgO (saturated KCl) electrode was used as the reference electrode and Ni-grid as the counter electrode. The specific capacitance was calculated from the discharge curves based on the following formula:

$$C_p = \frac{I\Delta t}{\Delta V} \qquad (1)$$

Here, C_p is the specific capacitance (F g^{-1}), I is the constant discharging current (A g^{-1}), Δt is the discharge time (s), and ΔV is the potential window during the discharge process (V), respectively.

3. RESULTS AND DISCUSSIONS

3.1 Composition and crystal structure of NiO-Co_3O_4 composites

The elemental composition of the prepared sample was studied by EDS spectrum, as shown in Figure 1. Evidently, the sample consists of Ni, Co and O. The chemical nature of the composites material is also confirmed by XRD, as shown in Figure 2. The diffraction peaks in curve A at 2θ = 37.2°, 43.3°, 62.9°, 75.4°, and 79.4° are corresponding to the (111), (200), (220), (311), and (222) planes, respectively, which can be indexed exactly to the cubic NiO phase (JCPDS no. 47-1049). Similarly, the diffraction peaks in curve C are in good agreement with the standard pattern of Co_3O_4 JCPDS no. 42-1467. The diffraction peaks suffer from a small shift in curve B compared with the curve A and C, due to the synergistic effect of NiO and Co_3O_4. Therefore, NiO and Co_3O_4 are co-existed in the composite and affect each other in the process of composite crystal growth.

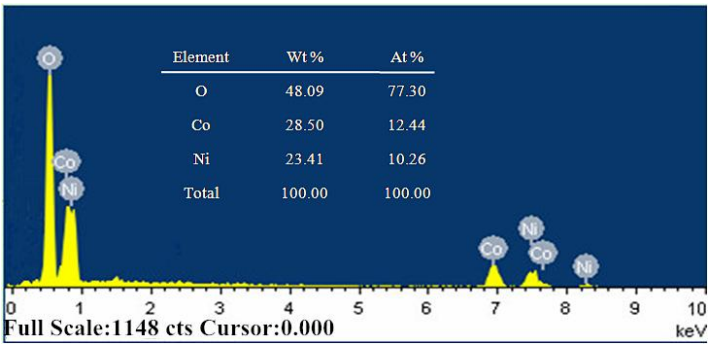

Figure 1. EDS of the prepared NiO-Co_3O_4 composite.

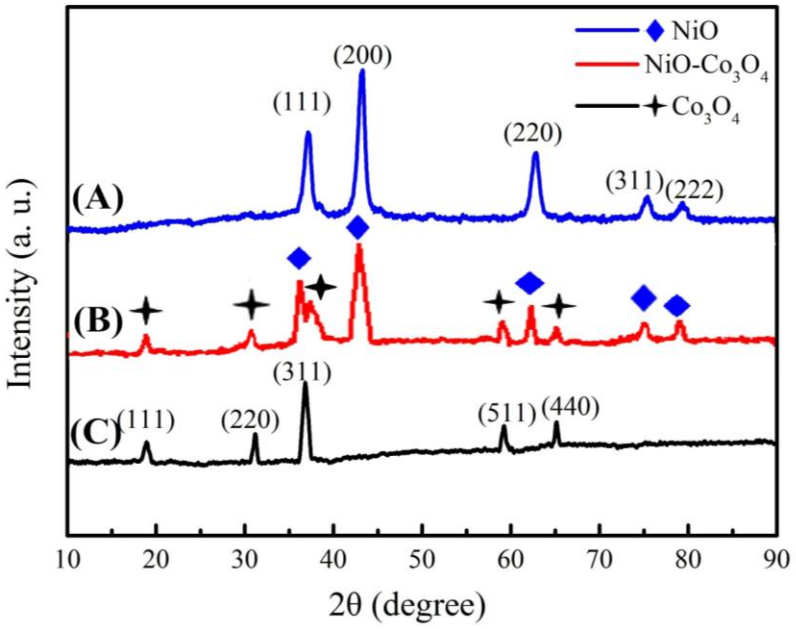

Figure 2. XRD patterns of the prepared NiO, NiO-Co_3O_4 and Co_3O_4.

3.2 Morphology

FE-SEM was used to examine the morphology of NiO-Co_3O_4 composites, as shown in Figure 3. It is clear that the composite is a 3D flower-like microsphere, which consists of cross-linked nanosheets, as shown in the low-magnification image (Figure 3(a)), indicating the robustness of the structure [8,25]. High-magnification SEM images as display in Figure 3(b-d) further reveal that hierarchical microspheres are assembled from 2D thin nanosheets with an average thickness of 20 nm. Meanwhile, the surface is coarse and porous, which suggests a highly porous texture.

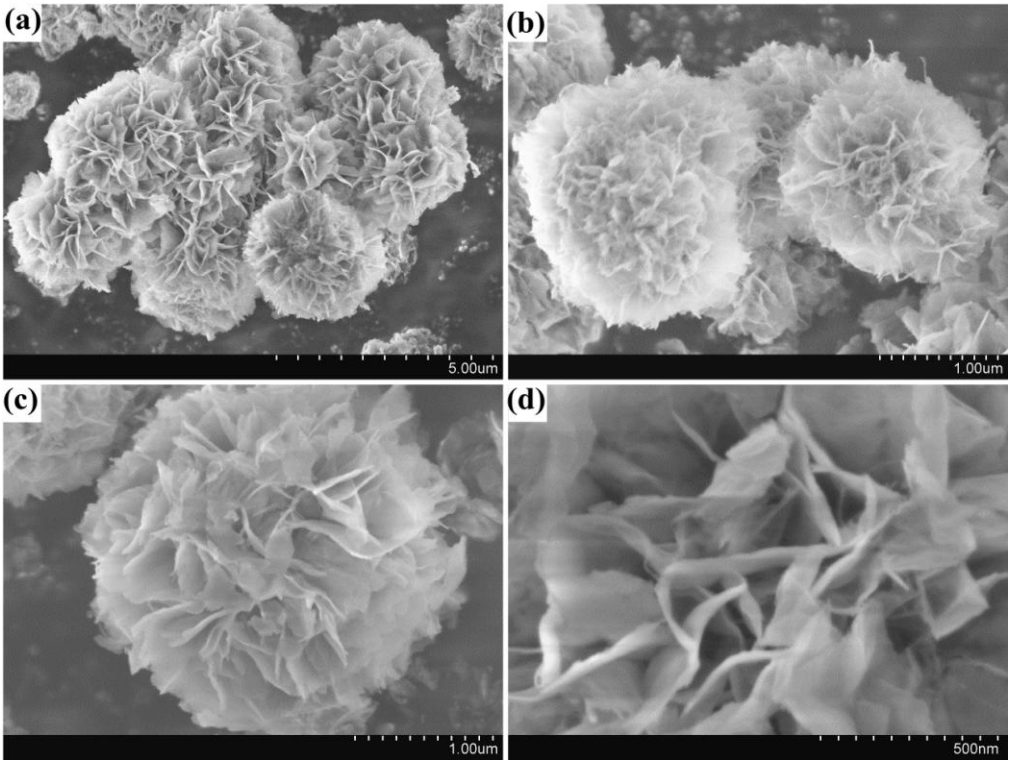

Figure 3. Low-magnification (a) and high-magnification (b-d) FESEM images of NiO-Co_3O_4.

3.3 Electrochemical properties

Figure 4(a) are recorded from the NiO-Co_3O_4 composite at scan rates of 5, 10, 20, 30, 40 and 50 mV s^{-1} in 6 mol L^{-1} KOH solution. A couple of redox peaks are observed within the potential windows ranging from -0.3 to 0.5 V, and these peaks result from the redox reactions related to M-O/M-O-OH, where M represents Ni or Co ions as follows [12,13,15]:

$$NiO + OH^- \rightarrow NiOOH + e^- \quad (2)$$

$$Co_3O_4 + OH^- + H_2O \rightarrow 3CoOOH + e^- \quad (3)$$

$$CoOOH + OH^- \rightarrow CoO_2 + H_2O + e^- \quad (4)$$

A pair of distinctive peaks at 0.18 and 0.00V can be clearly observed in the positive and negative sweep at 5 mV s^{-1}. Interestingly, the oxidation and reduction peaks shifted regularly toward higher and lower potentials, respectively, with increasing the sweep rate. This may be ascribed to the thesis that a high scan rate prevents the accessibility of ions from entering into the pores, and thus the transport of ions is limited (due to their slow diffusion) and only the outer surface could be utilized for the charge storage [9,27].

Galvanostatic charge-discharge profiles are presented in the potential range of 0-0.35 V in Figure 4(b). It can be seen that the profiles of all the curves have two obvious plateaus during charge-discharge process and these plateaus match well with two redox couples peaks observed in the CV curves. The sloped curve is characteristic of typical pseudocapacitance, originating from electrochemical adsorption-desorption or a redox reaction on the electrode/electrolyte interface [28]. The specific capacitances of the sample can be calculated by Formula (1). The NiO-Co_3O_4 as electrode

material exhibits extreme large pseudocapacitance of 1988.6, 1954.3, 1874.3, 1714.5 and 1491.4 F g^{-1} at discharge current densities of 1, 2, 5, 10 and 15 A g^{-1}, respectively, as shown in Figure 4(c). It is worth mentioning that the specific capacitance of the NiO-Co_3O_4 composite is much higher than that of reported NiO- and Co_3O_4- based electrode materials, especially at high scan rates [9,21,28,29].

Cycle stability is an important property for the application. Figure 4(d) shows the stability curve of the prepared NiO-Co_3O_4 electrode at a current density of 10 A g^{-1} for 1500 repetitive cycles. It can be seen that the specific capacitance decreases slightly after 1500 cycles. The capacitance only reduces 6.0%, indicating an excellent stability of the NiO-Co_3O_4 composite material.

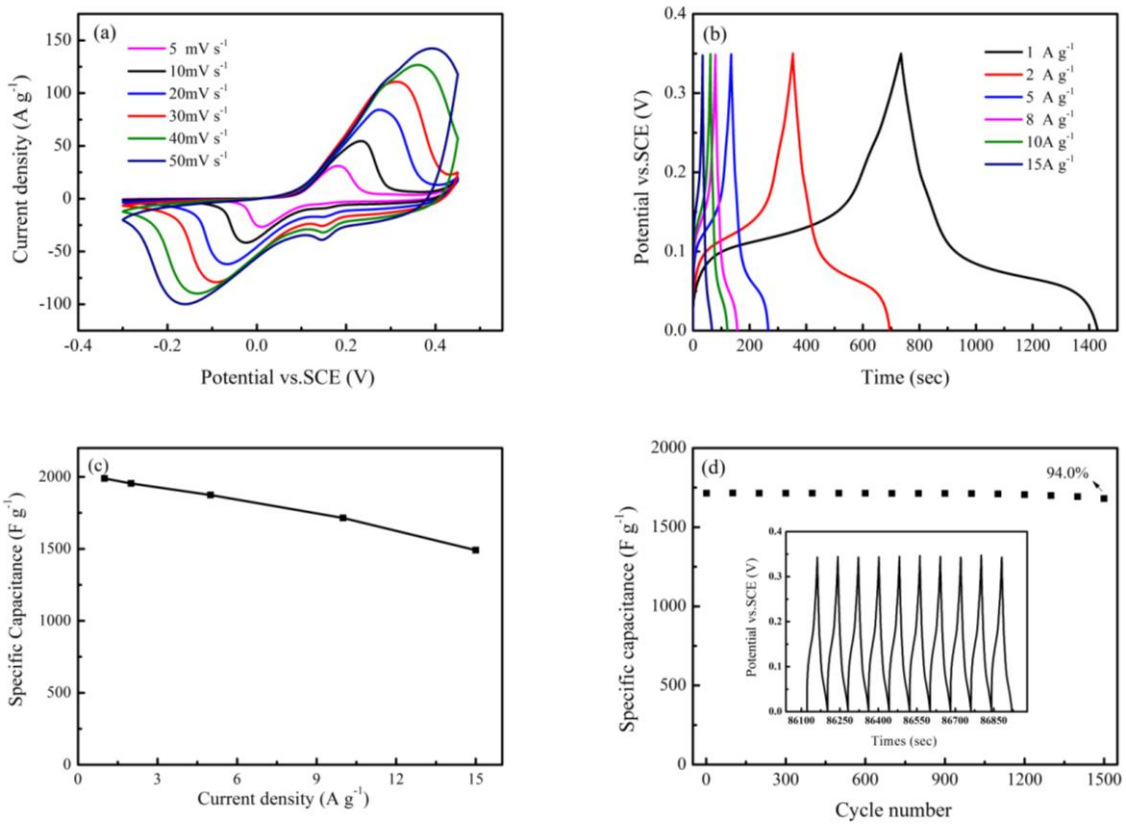

Figure 4. The electrochemical measurements of NiO-Co_3O_4 composite in 6 mol L^{-1} KOH electrolyte. (a) CV curves at various scan rates, (b) Galvanostatic charge-discharge curves at various current densities, (c) Specific capacitances at various current densities, (d) 1500 cycles charge-discharge at 10 A g^{-1}. The insert shows the last 10 cycles of charge-discharge.

The electrochemical impedance spectroscopy (EIS) of NiO-Co_3O_4 composite electrode is also further investigated. Nyquist plots of the EIS spectra of the electrode before/after 1500 cycles are shown in Figure 5. The axis intercepts in the high frequency range corresponds to the internal resistance (R_s), while the diameter of the semicircle represents the interfacial charge-transfer impendence (R_{ct}). Besides, the slopes of the straight line in the low-frequency indicate the values of the Warburg resistance (W) [31]. All of the above values are very small and almost no change after 1500

cycles, revealing good electronic conductivity, excellent capacitive behaviors and high stability of the NiO-Co_3O_4 composite.

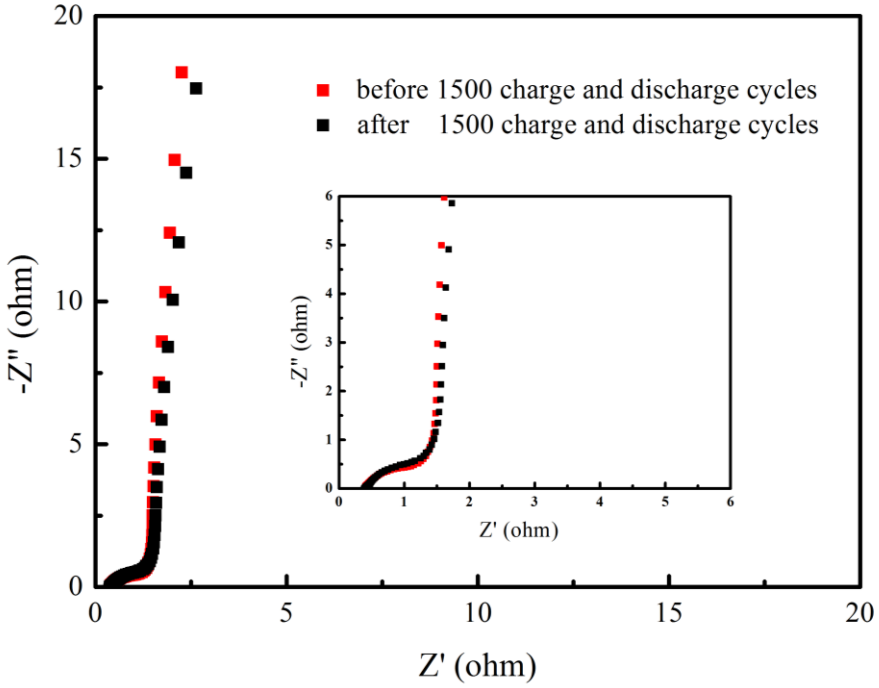

Figure 5. Electrochemical impedance spectra of NiO-Co_3O_4 electrode in the frequency range from 0.01 Hz to 100 kHz before and after 1500 cycles. The insert shows the enlarged EIS spectra.

This outstanding electrochemical performances can be attributed to the morphological characteristics of the porous and ultrathin nanosheets self-assembling into flower-like architectures, as well as the rational composition of the two constituents (NiO and Co_3O_4), which not only shortening the diffusion path for both electrons and ions, but also can take advantage of the synergistic effect of NiO and Co_3O_4 [9].

3.4 Influence of calcination temperature

The nitrogen adsorption-desorption isotherms at 77 K of the prepared T1, T2, T3 and the corresponding pore size distributions are calculated by Barrett-Joyner-Halenda (BJH) method, as displayed in Figure 6. It is clear that all three samples have a Type-IV isotherm with hysteretic loop at high relative pressures [12]. A well-defined Type H-3 hysteresis loop is observed in the region of P/P_0 from 0.7 to 1.0, suggesting the existence of mesopores, which can be further verified from BJH pore size distribution in Figure 6(d-f) [21,25]. The surface area and porous parameters are derived from the isotherms and tabulated in Table 1. The BET specific surface area, average pore size and total pore volume are all in the orders of T2 > T1 > T3. For T2, which has the largest surface area of 68.4 m^2 g^{-1},

displays a narrow and ordered pore-size distribution at ~ 5.4 nm. However, T1 (51.8 m^2 g^{-1}) reveals a sharp peak at ~ 5.6 nm and a wide peak at 11.8 nm, also T3 (43.4 m^2 g^{-1}) exhibits sharp peaks at ~ 3.3 and 5.6 nm and a wide peak at 15.9 nm. Due to the differences of BET specific surface area, pore size distribution and pore volume, it is logical to speculate that the NiO-Co_3O_4 composite prepared by different calcination temperatures will take on different electrochemical performances.

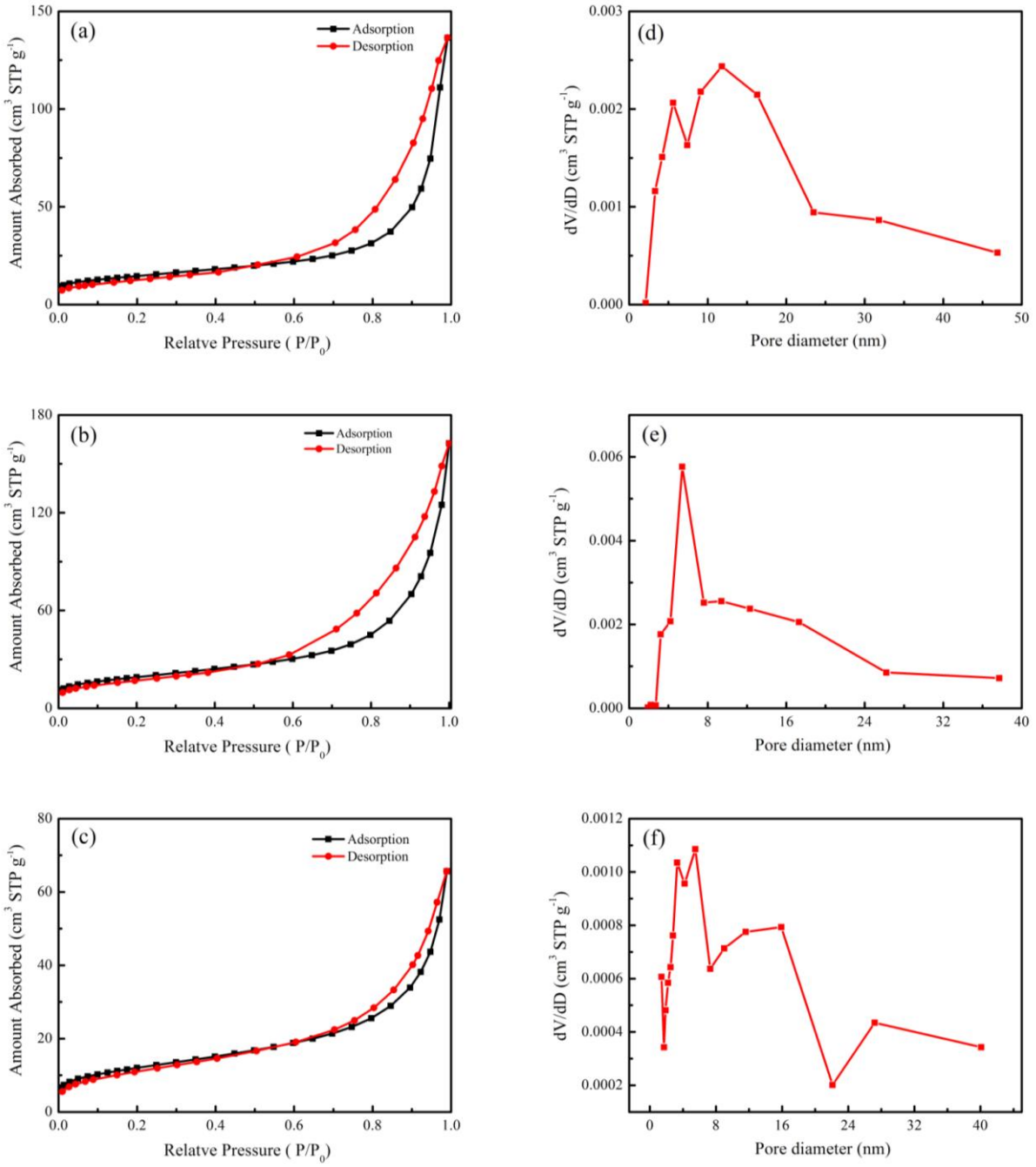

Figure 6. Nitrogen adsorption-desorption isotherms of (a) T1, (b) T2, (c) T3 and their corresponding pore size distributions (d), (e), (f).

Table 1. The surface area and porous parameters of T1, T2, T3.

Samples	BET specific surface area ($m^2 g^{-1}$)	Average pore size (nm)	Total pore volume ($cm^3 g^{-1}$)
T1	51.8	7.6	0.19
T2	68.4	5.4	0.25
T3	43.4	8.5	0.10

To estimate the properties of the NiO-Co_3O_4 prepared by different calcination temperatures, the comparison of the electrochemical performances are presented in Figure 7. The representative CV curves of the three samples at 5 mV s^{-1} were shown in Figure 7(a), from which we can conclude that the order of the area under the CV curve is T2 > T1 > T3. It is well-known that the specific capacitance is proportional to the area of the CV curve [13, 23]. Hence, the order of the specific capacitance is T2 > T1 > T3, which can be further confirmed by the following charge-discharge measurements.

Figure 7 (b) reveals the galvanostatic charge-discharge curves of the three electrodes at 1 A g^{-1} in the potential range of 0-0.35V. The specific capacitance of the materials can be calculated by Formula [1]. The specific capacitances of T1, T2, T3 are 1763.1, 1988.6, 1697.1 F g^{-1} at 1 A g^{-1}, respectively. The result is in good agreement with that of CV.

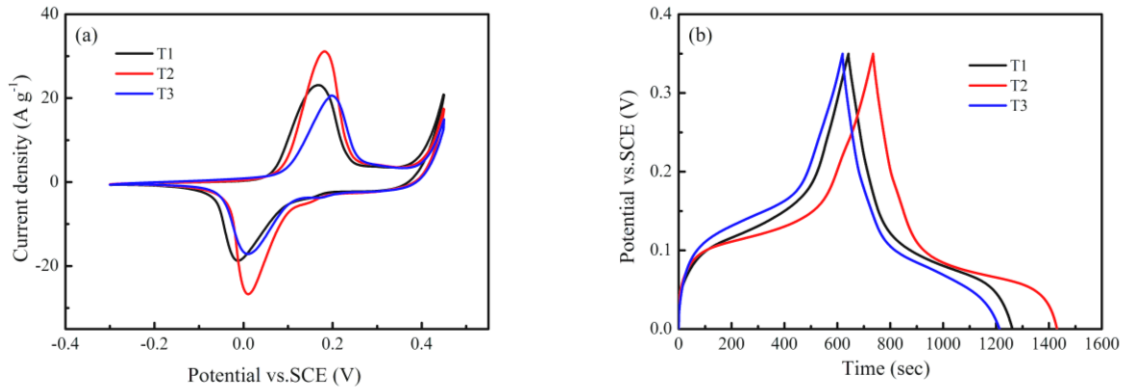

Figure 7. (a) CV curves at a scan rate of 5 mV s^{-1} and (b) charge-discharge curves of at a current density of 1 A g^{-1} of .T1, T2, T3.

The specific capacitances as a function of current densities are shown in Figure 8. All the specific capacitances are in orders of T2 > T1 >T3 at the same current densities. The capacity retention rates are 65.3%, 75.0%, 55.9%, respectively, as discharge current density increasing from 1 to 15 A g^{-1}. Therefore, T2 displays the best capacitive behaviors, suggesting that 350 °C is the optimal calcination temperature. It can be attributed to the highest BET specific surface area, largest pore volume and proper pore size distribution of T2, as shown in Table 1 and Figure 6, which can provide more active sites, and facilitate the electrolyte ion diffusion and charge transfer for fast faradaic redox reaction [24].

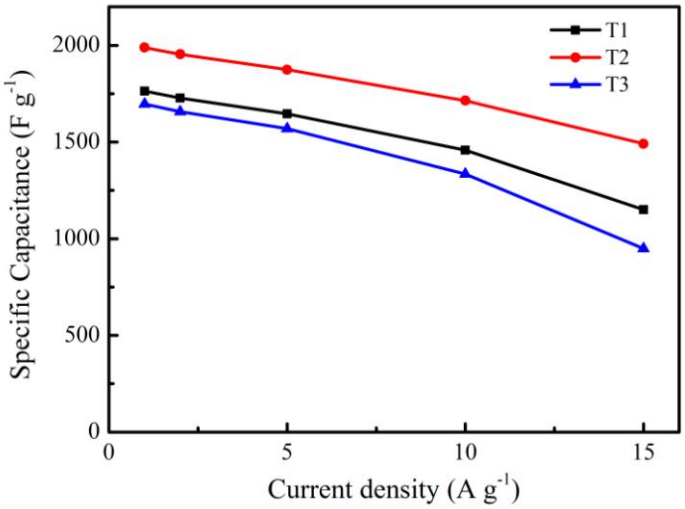

Figure 8. Specific capacitances of T1, T2, T3 at different current densities.

4. CONCLUSIONS

In summary, novel 3D hierarchical NiO-Co_3O_4 composites are synthesized with L-lysine as chelating agent. It is found that calcination temperature has an important effect on the properties of the prepared sample. The NiO-Co_3O_4 composite prepared at the optimal temperature 350 °C possesses a large amount mesopores, high BET surface area and large pore volume. The electrochemical characterizations manifest that the optimal sample shows an exceptionally high specific capacitance of 1988.6, 1954.3, 1874.3, 1714.5 and 1491.4 F g^{-1} at discharge current densities of 1, 2, 5, 10 and 15 A g^{-1}, respectively, with excellent cycling stability (retain 94.0 % after 1500 cycles at 10 A g^{-1}). The outstanding electrochemical performance is attributed to the desirable composition and the unique 3D hierarchical mesoporous flower-like architecture. The novel NiO-Co_3O_4 composite could be a competitive electrode material for the application in supercapacitors.

ACKNOWLEDGEMENTS
This work is financially supported by Tongji University Research Foundation (1380219039). The authors would like to thank the colleagues from the Chemistry Experimentation Center of Tongji University for their assistance in the sample characterizations.

References

1. J. H. Zhu, J. Jiang, Z. P. Sun, J. S. Luo, Z. X. Fan, X. T. Huang, H. Zhang and T. Yu, *Small*, 14 (2014) 2937.
2. J. Jiang, Y. Y. Li, J. P. Liu, H. T. Huang, C. Z. Yuan and X. W. Lou, *Adv. Mater.*, 24 (2012) 5166.
3. G. Wang, L. Zhang and J. Zhang, *Chem. Soc. Rev.*, 41 (2012) 797.
4. B. E. Conway, Electrochemical Supercapacitors: Scientific Fundamentals and Technological Applications, Kluwer Academic/Plenum Publishers, New York, 1999.
5. C. Liu, F. Li, L. P. Ma and H. M. Cheng, *Adv. Energy. Mater.*, 22 (2010) E28.
6. G. Q. Zhang and X. W. Lou, *Adv. Mater.*, 25 (2013) 976.

7. Z. Y. Lu, Q. Yang, W. Zhu, Z. Chang, J. F. Liu, X. M. Sun, D. G. Evans and X. Duan, *Nano Res.*, 5 (2012) 369.
8. Y. G. Liu, Y. Y. Zhao, Y. L. Yu, J. P. Li, M. Ahmad and H. Y. Sun, *New J. Chem.*, 38 (2014) 3084.
9. K. B. Xu, R. J. Zou, W. Y. Li, Y. F. Xue, G. S. Song, Q. liu, X. J. Liu and J. Q. Hu, *J. Mater. Chem. A*, (1) 2013 9107.
10. L. L. Peng, X, Peng, B, R, Liu, C, Z, Wu, Y, Xie and G. H. Yu, *Nano Lett.*, 13 (2013) 2151.
11. W. Tang, Y. Y. Hou, X. J. Wang, Y. Bai, Y. S. Zhu, H. Sun, Y. B. Yue, Y. P. Wu, K. Zhu and R. Holze, *J. Power Sources*, 197 (2012) 330.
12. D. M. Du, Z. H. Hu, Y. F. Liu, Y. H. Deng and J. M. Liu, *J. Aollys Comp.*, 589 (2014) 82.
13. K. Liang, X. Z. Tang and W. C. Hu, *J. Mater. Chem.*, 22 (2012) 11062.
14. Y. Teng, Z. X. Song, L. B. Wang and J. Xia, *J. Phys. Chem. C*, 118 (2014) 4767.
15. M. X. Liao, Z. H. Hu, Y. F. Liu and Q. Yu, *J. Aollys Comp.*, 562 (2013) 106.
16. E. Khoo, J. M. Wang, J. Ma and P. S. Lee, *J. Mater. Chem.*, 20 (2010) 8368.
17. I. Shakir, Z. Ali, J. Bae, J. J. Park and D. J. Kang, *Nanoscale*, 6 (2014) 4125.
18. C. Zhou, Y. W. Zhang, Y. Y. Li and J. P. Liu, *Nano Lett.*, 13 (2013) 2078.
19. A. K. Mondal, D. W. Su, Y. Wang, S. Q. Chen, Q. Liu and G. X. Wang, *J. Aollys Comp.*, 582 (2014) 522.
20. L. J. Xie, K. X. Li, G. H. Sun, Z. G. Hu, C. X. Lu, J. L. Wang and C. M. Zhang, *J Solid State Electrochem.*, 17 (2013) 55.
21. M. Huang, F. Li, J. Y. Ji, Y. X. Zhang, X. L. Zhao and X. Gao, *CrystEngComm*, 16 (2014) 2878.
22. Y. F. Yuan, X. H. Xia, J. B. Wu, X. H. Huang, Y. B. Pei, J. L. Yang and S. Y. Guo, *Electrochem. Commun.*, 13 (2011) 1123.
23. M. Li, S. H. Xu, Y. P. Zhu, P. X. Yang, Z. W. Wang and P. K. Chu, *J. Aollys Comp.*, 589 (2014) 364.
24. Y. R. Zhu, X. B. Ji, Z. P. Wu, W. X. Song, H. H. Hou, Z. B. Wu, X. He, Q. Y. Chen and C. E. Banks, *J. Power Sources*, 267 (2014) 888.
25. H. B. Wu, H. Pang and X. W. Lou, *Energy Environ. Sci.*, 6 (2013) 3619.
26. X. Wang, X. Han, M. Lim, N. Singh, C. L. Gan, M. Jan and P. S. Lee, *J. Phys. Chem. C*, 116 (2012) 12448.
27. W. W. Liu, C. X. Lu, K. Liang and B. K. Tay, *J. Mater. Chem. A*, 2 (2014) 5100.
28. X. Zhang, Y. Q. Zhao and C. L. Xu, *Nanoscale*, 6 (2014) 3638.
29. X. H. Xia, J. P. Tu, Y. Q. Zhang, X. L. Wang, C. D. Gu, X. B. Zhao and H. J. Fan, *ACS Nano*, 6 (2012) 5531.
30. X. Xu, H. Zhou, S. J. Ding, J. Li, B. B. Li and D. M. Yu, *J. Power Sources*, 267 (2014) 641.
31. Y. F. Zhang, M. Z. Ma, J. Yang, H. Q. Huang and X. C. Dong, *Nanoscale*, 6 (2014) 4303.